Available online at www.sciencedirect.com

ScienceDirect

Procedia Structural Integrity 7 (2017) 50–57

Structural Integrity Procedia

www.elsevier.com/locate/procedia

3rd International Symposium on Fatigue Design and Material Defects, FDMD 2017, 19-22 September 2017, Lecco, Italy

Microstructure and preliminary fatigue analysis on AlSi10Mg samples manufactured by SLM

C.A. Biffi[a]*, J. Fiocchi[a], P. Bassani[a], D.S. Paolino[b], A. Tridello[b], G. Chiandussi[b], M. Rossetto[b] and A. Tuissi[a]

[a] *National Research Council; Institute of Condensed Matter Chemistry and Technologies for Energy, Unit of Lecco, CNR ICMATE; Via G. Previati 1E, 23900 Lecco, Italy.*

[b] *Politecnico di Torino, Department of Mechanical and Aerospace Engineering, Corso Duca degli Abruzzi 24, 10129 Turin, Italy*

Abstract

Nowadays, selective laser melting (SLM) is considered as the most challenging technology for manufacturing complex components in different industrial fields, such as biomedical, aerospace and racing. It is well-known that SLM may yield to microstructures significantly different from those obtained by conventional casting, thus affecting the mechanical properties of the component.

In the present paper, microstructural and mechanical tests were carried out on AlSi10Mg samples manufactured by SLM technique in the XY building configuration. Homogeneous composition and typical microstructures were achieved for all the investigated samples. The mechanical properties were assessed through a tensile test and through the Impulse Excitation Technique (IET). The feasibility of ultrasonic Very High Cycle Fatigue (VHCF) tests with Gaussian specimens characterized by large loaded volumes (risk-volumes) was also experimentally verified in the paper. A Gaussian specimen was designed and manufactured. A preliminary ultrasonic test was then carried out on the manufactured specimen and the fracture surface was finally investigated.

Peer-review under responsibility of the Scientific Committee of the 3rd International Symposium on Fatigue Design and Material Defects.

* Corresponding author.

E-mail address: carloalberto.biffi@cnr.it

2452-3216

Peer-review under responsibility of the Scientific Committee of the 3rd International Symposium on Fatigue Design and Material Defects.

10.1016/j.prostr.2017.11.060

Keywords: Additive manufacturing; selective laser melting; AlSi10Mg; microstructure; mechanical testing; very-high-cycle fatigue.

1. Introduction

The production of components through Additive Manufacturing (AM) processes is becoming increasingly attractive for industrial applications, as far as AM permits to manufacture complex geometries, which could be hardly obtained by conventional machining and manufacturing processes. Moreover, AM permits to manufacture components without strong geometrical constraints and permits for a significant material savings thanks to the lack of scraps. Among AM techniques for metals, Selective Laser Melting (SLM) is one of the most used and attractive techniques: the component is build layer by layer by melting with a laser beam (Herzog et al., 2016) the material powder, deposited in a uniform bed. The production of aluminum parts by SLM is nowadays of utmost interest, due to the large use of this material in many demanding industrial fields, such as the automotive and aeronautical industry (Olakanmi et al., 2015). Aluminum alloys, currently used for AM, are mainly Si-based alloys, characterized by good castability, low shrinkage and relatively low melting temperature. In particular, the AlSi10Mg with a nearly eutectic composition is currently widely adopted for SLM processes and its microstructural and mechanical properties have been extensively analyzed and investigated in the literature (Lam et al.,2015; Thijs et al., 2013; Brandl et al., 2012; Buchbinder et al., 2011). Strong efforts have been made in recent years to optimize the SLM process parameters, in order to obtain full dense aluminum parts (Buchbinder et al., 2011; Read et al., 2015; Aboulkhair et al., 2014; Rao et al., 2016) and to define the proper thermal treatments (Fiocchi et al., 2017; Aversa et al., 2017) allowing for enhancing the mechanical properties. In this respect, several experimental tests were performed in the literature to assess the mechanical properties (static properties, fatigue response (Aboulkhair et al., 2016; Siddique et al., 2015; Maskery et al., 2015) and corrosion resistance (Cabrini et al., 2016)) of AlSi10Mg parts manufactured through the SLM process.
In the present paper, microstructural and mechanical tests were carried out on AlSi10Mg specimens manufactured through SLM process in the XY configuration, according to the ISO/ASTM 52900:2015 (E) Standard. Scanning Electron Microscopy (SEM) analyses were carried out to analyze the composition and the microstructure obtained through the selected SLM process parameters. The mechanical properties were assessed by means of a tensile test and the Impulse Excitation Technique (IET). The feasibility of ultrasonic Very High Cycle Fatigue (VHCF) tests with Gaussian specimens (Tridello et al., 2013) was also verified in the paper. The Gaussian shape was recently proposed at the Politecnico di Torino: the specimen profile is described by a Gaussian function which ensures a uniform stress distribution and permits to test risk-volumes (volume of material subjected to a stress amplitude larger than the 90% of the maximum applied stress, according to (Murakami et al., 2002) and (Furuya et al., 2011) significantly larger than those of hourglass and dog-bone specimens, which are commonly adopted in the literature. According to the statistical dependency between the defect size and the risk-volume, tests on large risk-volumes allow for a more proper assessment of the VHCF response. A Gaussian specimen with V_{90} equal to $2300\ \mathrm{mm}^3$ was designed and manufactured through SLM. A preliminary ultrasonic VHCF test was carried out on the Gaussian specimen and the fracture surface was finally investigated to assess the crack origin.

2. Materials and Methods

In this Section, the material and the experimental activity are described in detail. In particular, in Section 2.1, the AlSi10Mg properties and the SLM process parameters are reported. In Section 2.2, a Gaussian specimen with V_{90} equal to $2300\ \mathrm{mm}^3$ is designed and the testing configuration for the preliminary ultrasonic test is described.

2.1. Material and SLM Process

Gas atomized AlSi10Mg powders, whose chemical composition is reported in Table 1, were processed. The powder featured a particles size between 20 μm and 63 μm, with average size of approximately 45 μm.

Table 1. Chemical composition of the AlSi10Mg powder (wt. %)

Si	Mg	Cu	Ni	Fe	Mn	Ti	Al

10	0.4	< 0.25	< 0.05	< 0.25	< 0.1	< 0.15	bal.

An SLM Solutions (model 500 HL quad 4 × 400 W) Selective Laser Melting system, equipped with 4 continuous wave ytterbium fiber lasers, was used to manufacture the samples for the microstructural and mechanical tests. In particular, seven rectangular bars (10 mm × 10 mm × 50 mm) for the microstructural analysis and the IET tests, standard dog-bone specimens for the tensile tests and a Gaussian specimen for the ultrasonic test (Fig. 1) were manufactured. The tests were performed in the as built condition.
The process parameters are reported in Table 2. Scanning strategy was kept constant during the manufacturing process: each scanning section is rotated by 67° with respect to the previous one and the scheme is repeated every 180 layers.

Table 2 Process parameters used in the SLM building of the AlSi10Mg samples

Power	Building plate temperature	Scanning speed	Spot size	Hatch distance	Layer thickness	Atmosphere
350 W	150 °C	1.15 m/s	80 μm	170 μm	50 μm	Argon

The microstructural features of the investigated samples were assessed by using the Scanning Electronic Microscope (SEM model Leo 1413) and the Field Emission Microscope (FEG-SEM SU70 Hitachi, equipped with an EDX probe analysis). The static mechanical properties were assessed through tensile tests at room temperature (strain rate of 0.015 min^{-1}) by using a MTS 2/M machine, equipped with extensometer for measuring the strain during the tests.

2.2. VHCF test: Gaussian specimen and experimental setup

The feasibility of ultrasonic VHCF tests with a Gaussian specimen was also verified in the paper. A Gaussian specimen with $V_{90} = 2300\ mm^3$ was designed according to the procedure described in Paolino et al. (2014). The material properties considered for the specimen design were experimentally assessed. The dynamic elastic modulus, E_d, was assessed through IET by using five rectangular bars with the geometry reported in Section 2.1. According to the ASTM Standard E1876-09, the bars, supported at the half of their length, were hit at one of the free ends by using a small hammer. At the other end, the vibration amplitude was acquired by using a microphone. The acquired signal, properly amplified, was used for assessing the first longitudinal resonance frequency of the bar and for computing E_d according to the ASTM Standard E1876-09. Table 3 reports the measured E_d values for the five rectangular bars. In the Table, the material density, ρ, is also reported. For the computation of ρ, the mass was measured by using a high-resolution digital balance, whereas the volume was computed by considering the actual dimensions of each bar measured by using a digital caliber (resolution 0.01 mm).

Table 3: Measured values of E_d and ρ.

	Test 1	Test 2	Test 3	Test 4	Test 5
E_d [GPa]	72	72.2	72.5	70.8	71.9
ρ [kg/m^3]	2625	2630	2639	2600	2634

According to Table 3, the E_d and the ρ values were in a small range ([70.8;72.5] GPa for E_d and [2600;2639] kg/m^3 for ρ), thus showing that the process parameters permitted to obtain repeatable mechanical properties. In particular, for the Young's modulus the limited scatter found through IET is within the range of scatter ($\pm$ 5 GPa) reported in the literature (Aboulkhair et al., 2016.; Kempen et. al, 2012). For the design of the Gaussian specimen, the average value between the five measurements was considered. A Gaussian specimen with $V_{90} =$

2300 mm^3 was analytically designed and verified through Finite Element Analysis (FEA). Fig. 1 reports the geometry of the Gaussian specimens designed for the experimental test.

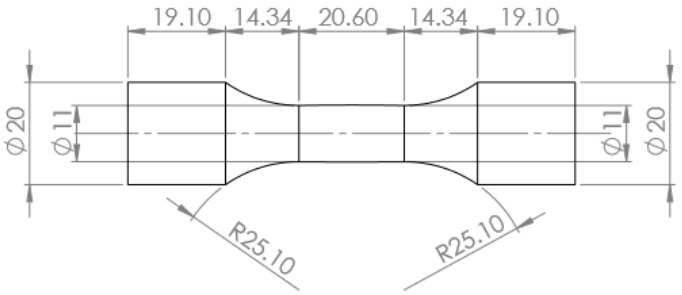

Fig. 1: Geometry of the Gaussian specimens used for the VHCF test.

The specimen was finally manufactured with a uniform allowance of 0.1 mm and finely polished by using sandpapers with increasing grit (from 240# to 1200#) in order to remove the residual parts of the support structures and macroscopic surface defect. Fig. 2 shows the Gaussian specimen in the as built condition (Fig. 2a) and after the polishing process (Fig. 2b).

(a) (b)

Fig. 2: Gaussian specimen for the VHCF test: (a) specimen in the as-built condition; (b) specimen after polishing.

Ultrasonic fatigue tests at constant stress amplitude were performed by using the ultrasonic testing machine developed at the Politecnico di Torino (Tridello et al., 2015). A closed loop control, based on the strain amplitude measured at the specimen center through a T-rosettes strain gages (HBM 1-XY311.5/350), was used to keep the stress constant during the test. Three vortex tubes were used for cooling the specimen. The temperature at the specimen mid-section, continuously monitored during the tests by using an infrared sensor, was maintained below 298 K. In order to induce an internal failure from a defect, the specimen was loaded in a variable amplitude loading condition, according to the following scheme:10^8 cycles with steps of 5 MPa, from 55 MPa to 75 MPa, 10^8 cycles at 85 MPa and up to failure at 95 MPa.

3. Results and Discussion

In this Section, the experimental results are described and discussed. In Section 3.1, the results of the microstructural analysis are analyzed. In Section 3.2, the ultimate stress is assessed from the stress-strain curve. Finally, in Section 3.3, the fracture surface of the Gaussian specimen is investigated to assess the origin of the fatigue crack.

3.1. Microstructural investigation

Fig. 3 shows four micrographs obtained by using the SEM: Fig. 3a and Fig. 3b shows the micrograph in the z direction (i.e., parallel to the building direction), respectively. Fig. 2c and 2d shows a micrograph in the XY plane,

(i.e. perpendicular to the building direction). The typical superposition of laser tracks, which was formed due to the layer by layer building strategy, is clearly visible. As expected, melt pools are half-cylindrical, along the z-direction, whereas they appear as elongated tracks in the XY plane. In both cases they are characterized by an inner fine fusion zone surrounded by a coarser heat affected zone. At higher magnification (Fig. 2b and 2d) the investigated alloy presented a cellular structure, consisting of an interconnected Si network dispersed within a α aluminium matrix. This microstructure, arising from the high cooling rates typical of the SLM process, is verified in the literature (Thijs et al., 2013) to positively affect the mechanical properties.

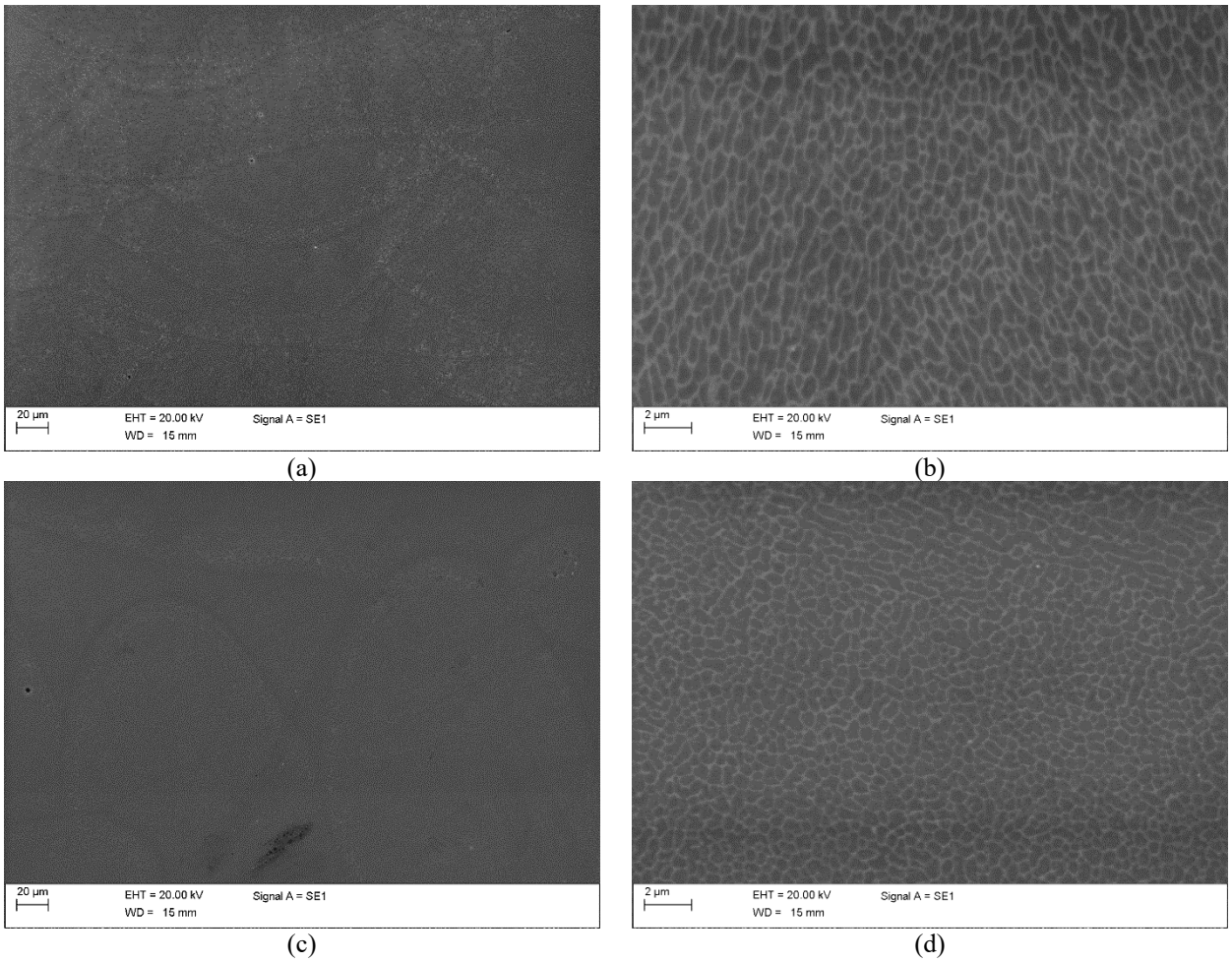

Fig. 3: SEM micrographs of SLM built samples: (a)XZ section at low magnification; (b) XZ section at high magnification (fine fusion zone); (c) XY section at low magnification; (d) XY section at high magnification (fine fusion zone).

3.2. Tensile test

Experimental tests were performed on samples built along XY plane, as far as this building configuration permits to attain higher and less dispersed mechanical properties. A tensile test on as-built dog-bone specimen confirmed the remarkable improvement of the mechanical properties induced by the SLM process. The sample showed a ductile behaviour (elongation at failure of about 5.5 %), with a yield strength of 287 MPa and an ultimate tensile strength of 414 MPa, about 100 MPa higher than the corresponding mechanical properties of an AlSi10Mg obtained by conventional casting (Kempen et al., 2012). Fig. 4 shows the stress strain curve obtained by testing the dog-bone

specimen.

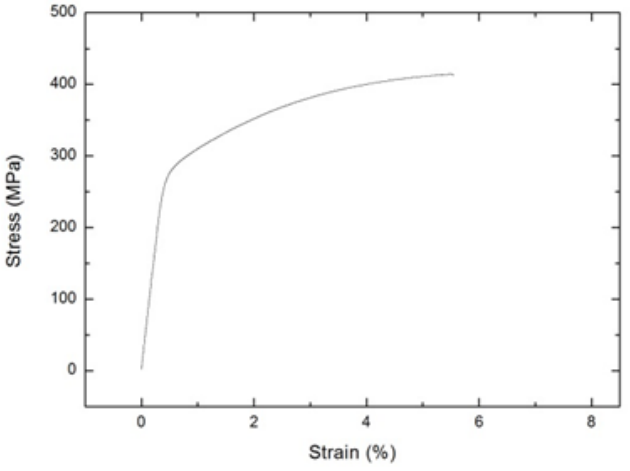

Fig. 4: Stress-strain curve of the as-built sample.

3.3. VHCF test

Following the load scheme reported in Section 2.2, the Gaussian specimen was tested up to failure, which occurred at 95 MPa at 1.98×10^6 cycles, after a total number of cycles equal to 6.02×10^8 cycles. Fig. 5 shows two images of the fracture surface taken at the optical microscope. Fig. 5a and Fig. 5b show a global view of the fracture surface and a magnification of the crack origin zone, respectively.

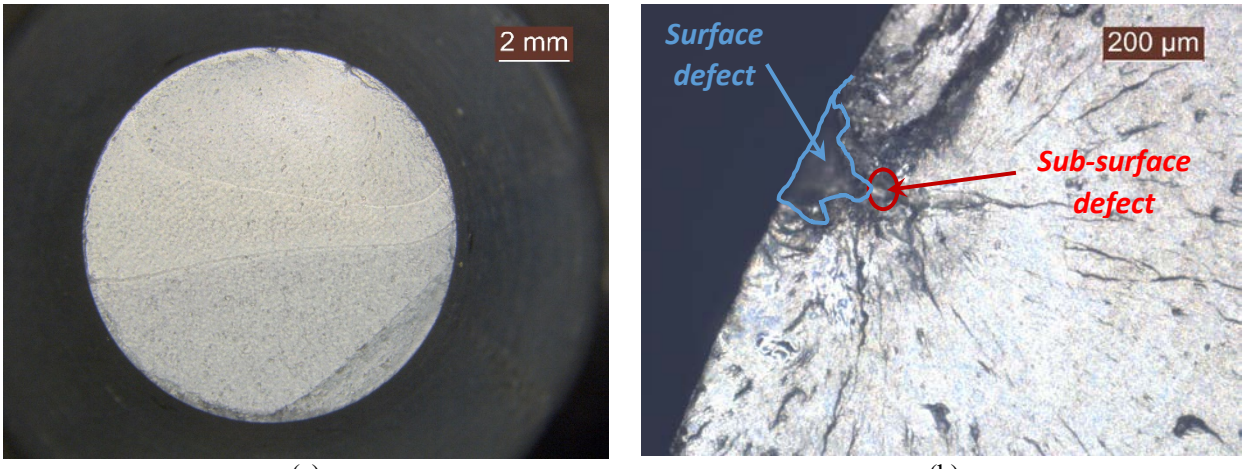

(a) (b)

Fig. 5: Optical images of the fracture surface: (a) global view; (b) magnification of the crack origin.

According to Fig. 5, the crack originated from two defects located near the specimen surface. The surface defect highlighted in blue probably originated during the support removal operations and was not eliminated in the polishing phase. The subsurface defect was investigated by using the field emission SEM. SEM micrographs of the fracture surface are collected in Fig. 6: Fig. 6a shows the crack initiation zone, Fig. 6b the crack propagation zone, Fig. 6c the transition zone between propagation and final fracture and Fig. 6d fractured brittle particles found in the final failure zone. Fig. 6a shows a magnification of the subsurface defect highlighted in Fig. 5b, which, through EDX analysis, was found to be aluminum oxide (Al_2O_3), which was either contained in the powder used for

production or came from the outside during surface finishing operations. Another possibility is that the oxide was formed during the manufacturing process (i.e., due to oxidized vapor or originated from the small oxide layer that could form around powder, according to Tang (2017)). Moreover, other areas with oxide defects were also found in proximity of the crack initiation point. By taking into account Fig. 6b, the crak propagated along a linear intergranular path inside the fine fusion zone of the melt pools, whereas a more irregular progression can be observed in the heat affected zones. The half-cylindrical shape of the melt pools can be observed in Fig. 6b. The final failure zone is clearly visible in Fig. 6c, even though the crack propagation is intergranular and leaves weak traces of the melt pool structure. The fracture zone (Fig. 6d) was finally investigated. Cleavage areas were noted in the failure zone, in proximity of internal spherical porosities or oxide particles, similar to the one that caused the crack initiation. (Fig. 6a).

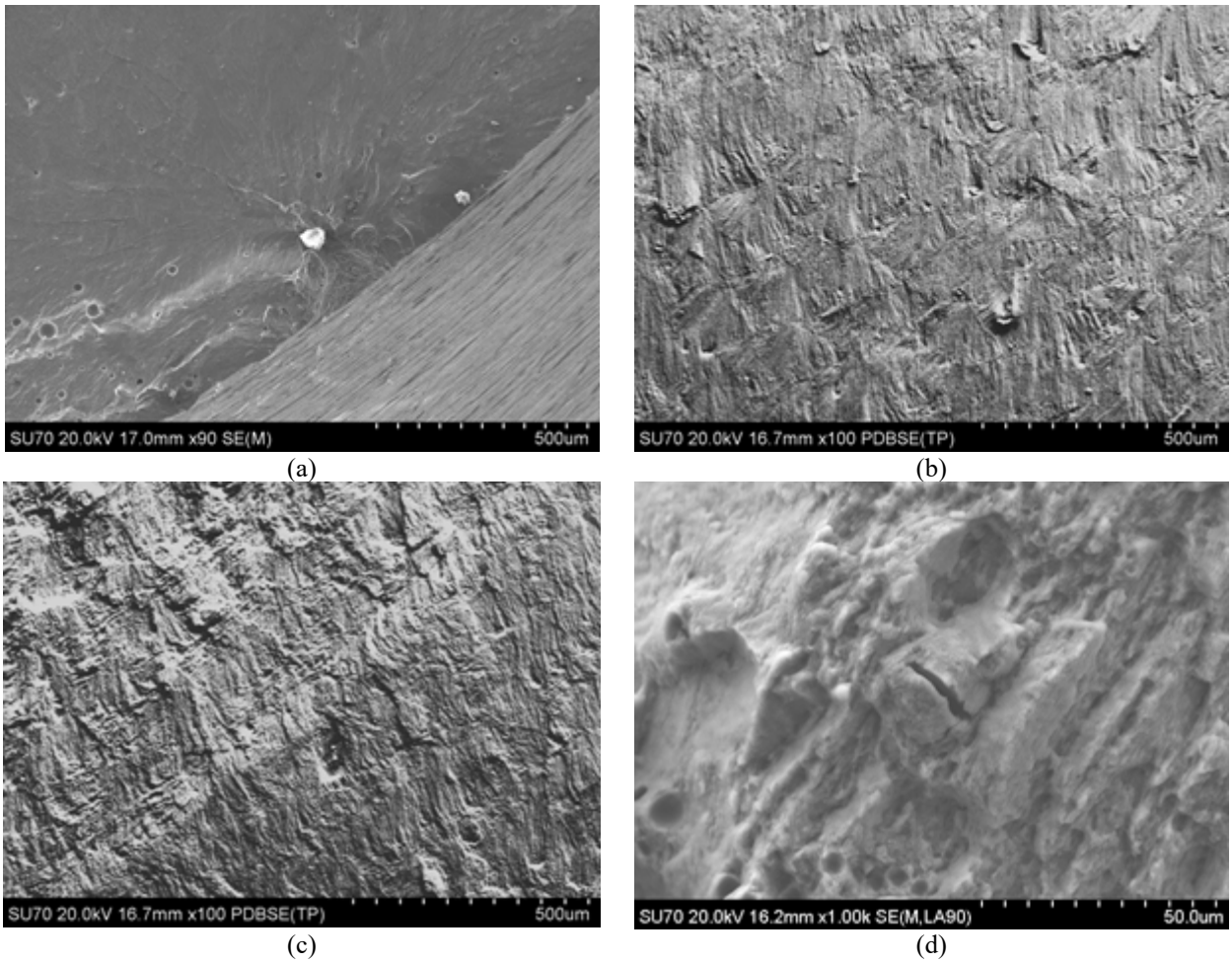

Fig. 6: SEM micrographs of the fracture surface: a) crack initiation zone; b) crack propagation zone; c) transition to final failure zone; d) brittle particles in the final failure zone.

4. Conclusions

In the present paper, preliminary microstructural and mechanical tests were carried out on AlSi10Mg specimens manufactured through SLM process in the XY configuration. Specimens were tested in the as-built condition. The microstructural analyses showed that the process parameters allowed for a homogenous microstructure similar to the

one described in literature. The tensile test confirmed the increment of the static mechanical properties in AlSi10Mg specimens produced through SLM process, as reported in the literature.

The feasibility of ultrasonic VHCF tests with large Gaussian specimens was also verified in the paper. A Gaussian specimen with a 2300 mm^3 risk-volume was designed and tested by using an ultrasonic fatigue testing machine. The specimen failed at more than 6×10^8 cycles, confirming that ultrasonic tests on large Gaussian specimen manufactured through SLM can be performed. Gaussian specimens could be effectively used for assessing the VHCF response as well as the defect size distribution of large volumes of SLM materials.

References

Herzog, D., Seyda, V., Wycisk, E., Emmelmann, C., 2016. Additive manufacturing of metals, Acta Materialia 117, 371–392.

Olakanmi, E.O., Cochrane, R.F., Dalgarno, K.W., 2015. A review on selective laser sintering/melting (SLS/SLM) of aluminum alloy powders: processing, microstructure and properties, Progress in Materials Science 74, 401-477.

Lam, L.P., Zhang, D.Q., Liu, Z.H., Chua, C.K., 2015. Phase analysis and microstructure characterisation of AlSi10Mg parts produced by Selective Laser Melting, Virtual Phys. Prototyp. 2759.

Thijs, L., Kempen, K., Kruth, J., Van Humbeeck, J., 2013. Fine-structured aluminium products with controllable texture by selective laser melting of pre-alloyed AlSi10Mg powder, Acta Materialia 61, 1809–1819.

Brandl, E., Heckenberger, U., Holzinger, V., Buchbinder, D., 2012. Additive manufactured AlSi10Mg samples using Selective Laser Melting (SLM): Microstructure , high cycle fatigue , and fracture behavior, J. Mater. 34, 159–169.

Buchbinder, D., Schleifenbaum, V., Heidrich,V., Bultmann, V., 2011. High Power Selective Laser Melting (HP SLM) of Aluminum Parts, Phys. Procedia. 12, 271–278.

Read, N., Wang, W., Essa, K., Attallah, V., 2015. Selective laser melting of AlSi10Mg alloy: Process optimisation and mechanical properties development, Materials and Design 65, 417–424.

Aboulkhair, N.T., Everitt, N.M., Ashcroft, I., Tuck, C., 2014. Reducing porosity in AlSi10Mg parts processed by selective laser melting, Additive Manufacturing 1, 77–86.

Rao, H., Giet, S., Yang, V., Wu, V., Davies, C.H.J., 2016. The influence of processing parameters on aluminium alloy A357 manufactured by Selective Laser Melting, Materials and Design 109, 334–346.

Fiocchi, J., Tuissi, A., Bassani, P., Biffi, C.A., 2017. Low temperature annealing dedicated to AlSi10Mg selective laser melting products, Journal of Alloys and Compounds, 695, 3402–3409.

Aversa, A., Lorusso, M., Trevisan, F., Ambrosio, E., Calignano, F. D. Manfredi, S. Biamino, P. Fino, M. Lombardi, M. Pavese, 2017. Effect of Process and Post-Process Conditions on the Mechanical Properties of an A357 Alloy Produced via Laser Powder Bed Fusion, Metals 7, 68.

Aboulkhair, N.T., Maskery, I., Tuck, C., Ashcroft, I., Everitt, N.M., 2016. Improving the fatigue behaviour of a selectively laser melted aluminium alloy: Influence of heat treatment and surface quality, Mater. Des. 104, 174–182.

Siddique, S., Imran, M., Wycisk, E., Emmelmann, C., Walther, F., 2015. Influence of process-induced microstructure and imperfections on mechanical properties of AlSi12 processed by selective laser melting, J. Mater. Process. Technol. 221, 205–213.

Maskery, I., Aboulkhair, N.T., Tuck, C., Wildman, R.D., Ashcroft, I.A., Everitt, N.M., Hague, R.J.M., 2015. Fatigue performance enhancement of selectively laser melted aluminium alloy by heat treatment, Solid Free. Fabr. Symp. 1017–1025.

M. Cabrini, S. Lorenzi, T. Pastore, S. Pellegrini, M. Pavese, P. Fino, E.P. Ambrosio, F. Calignano, D. Manfredi, 2016. Corrosion resistance of direct metal laser sintering AlSiMg alloy, Surf. Interface Anal. 48, 818–826.

ISO/ASTM 52900:2015(E) - Standard Terminology for Additive Manufacturing – General Principles – Terminology. Genève. International Standard,Organization (ISO), 2015.

Tridello, A., Paolino, D. S., Chiandussi, G., Rossetto, M., 2013. Comparison between dog-bone and Gaussian specimens for size effect evaluation in Gigacycle fatigue. Frattura e Integrità Strutturale 26, 49-56.

Murakami, Y., 2002. Metal Fatigue: Effects Of Small Defects And Nonmetallic Inclusions. Elsevier, Oxford.

Furuya, Y., 2011. Notable size effects on very high cycle fatigue properties of high strength steel. Mater. Sci. Eng. A 528, 5234–5240.

ASTM Standard E1876-09 (2009). Standard test method for dynamic Young's modulus, Shear modulus, and Poisson's ratio by impulse excitation of vibration. West Conshohocken (PA): ASTM International; 2009.

Tridello, A., Paolino, D. S., Chiandussi, G., Rossetto, M., 2015. VHCF response of AISI H13 steel: assessment of size effects through Gaussian specimens. Procedia Engineering 109, 121-127.

Aboulkhair, N.T., Maskery, I., Tuck, C., Ashcroft, I., Everitt, N.M. 2016. The microstructure and mechanical properties of selectively laser melted AlSi10Mg: The effect of a conventional T6-like heat treatment. Mater. Sci. Eng. A 667, 139-146

Kempen, K., Thijs, L., Van Humbeeck, J., Kruth, J.-P., 2012. Mechanical Properties of AlSi10Mg Produced by Selective Laser Melting, Phys. Procedia. 39, 439–446.

Tang, M., 2017. Inclusions, Porosity, and Fatigue of AlSi10Mg Parts Produced by Selective Laser Melting. Dissertations. 903. http://repository.cmu.edu/dissertations/903.